The Journal's name will be set by the publisher
DOI: will be set by the publisher

Design and status of the Mu2e experiment

Stefano Miscetti[1,a] on behalf of the Mu2e Collaboration

[1] *Laboratori Nazionali di Frascati dell'INFN, Via Enrico Fermi 40, 00044, Frascati, Italy*

Abstract. The Mu2e experiment aims to measure the charged-lepton flavor violating neutrino-less conversion of a negative muon into an electron in the field of a aluminum nucleus with the goal of improving by four orders of magnitude the previous measurement with similar technique. In the Standard Model, these process have negligible rates. However, in many of the Beyond the Standard Model scenarios, their rates are within the reach of the next generation of experiments. In this paper, we explain the sensitivity to new physics scale and the complementarity of approach and reach provided by MU2E with respect to Mu3e and MEG upgrade. For the conversion process, the signal will appear as a mono-energetic electron very close to the muon rest mass. The experimental technique will be explained as well as the status of design and construction of the experiment.

1 Introduction

In the Standard Model, SM, hadronic flavor transitions are allowed and the CKM matrix represents the probability for a quark of a specific family to turn into a different quark of another family. In the lepton sector, since SM neutrinos are massless, transitions between charged and neutral leptons preserve flavor. Nevertheless, flavor transitions between neutral leptons have been observed in neutrino oscillations that implies non conservation of lepton flavor number. Even assuming massive neutrinos, charged lepton flavor violation (CLFV) processes are extremely suppressed in the SM. The SM constraint on the branching ratio for $\mu \to e\gamma$ is $B(\mu \to e\gamma) \leq 10^{-52}$ [1]. Theories beyond the Standard Model, BSM, predict additional particles and interactions that can enhance such processes up to a measurable level (for a recent review see [2]).

Experimentally, the search for CLFV has a long history both in the muon, τ decays (for the processes $\mu \to e\gamma$, $\mu \to 3e$, $\tau \to \mu\gamma$, $\tau \to 3\mu$) and in the muon conversion processes, $\mu N \to eN$, in the presence of a nucleus. Started with pioneering measurements with cosmic rays in the late 1940, the sensitivity is improved by many orders of magnitude reaching stringent limits both for $\mu \to e\gamma$ (with BR$< 5.7 \times 10^{-13}$ at 90 % C.L.) [3] and for muon conversion on gold ($R_{\mu e} < 6 \times 10^{-13}$ [4]. An international program of CLFV searches exists. In the muon sector, there is the completion of the MEG experiment at PSI and its upgrade, MEG-II, the proposed Mu3e search at PSI and the searches for muon to electron conversion (Mu2e[5] at Fermilab, COMET at J-PARC). CLFV searches are of particular interest because of the possibility to carry out clean measurements which are free of theoretical background. In case of observation they indicate a clear evidence of physics beyond the standard model. In case of non observation they pose strong limits on the development of new theories.

[a] e-mail: Stefano.Miscetti@LNF.INFN.IT

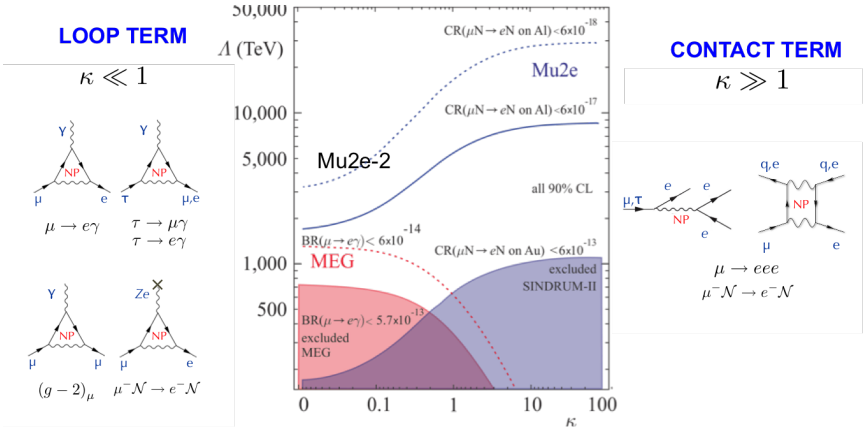

Figure 1. Sensitivity of $\mu \to e\gamma$, $\mu \to e$ transition and $\mu \to 3e$ to the scale of new physics Λ as a function of the parameter κ. The shaded areas are excluded by present limits. On the left (right) side, the dipole (four-fermion) diagrams are shown for the different processes.

A model independent description of the CLFV transitions, for physics beyond the Standard Model, is provided by an effective lagrangian [6] where the different processes are divided in dipole amplitudes and four-fermion, or contact term, operators. The $\mu \to e\gamma$ decay is mainly sensitive to the dipole amplitude, while $\mu \to e$ conversion and $\mu \to 3e$ receive contributions also from the four-fermion interactions. It is customary to parametrize the interplay between the two amplitudes by means of two parameters [6]: Λ, which sets the mass scale, and κ, which governs the ratio of the four fermion to the dipole amplitude. For $\kappa \ll 1 (\gg 1)$ the dipole-type (four-fermion) operator dominates. Figure 1 summarizes the power of different searches to explore this parameter space. A scale $\Lambda < 700$ TeV is already excluded by present limits, posing serious constraints on Standard Model extensions, supersymmetry in the first place. Nonetheless Λ is only an effective scale and is not immediately comparable to the mass M of new particles accessible by direct search at LHC in the TeV scale. The interpretation of a eventual direct observation of new physics at LHC will have to take into account precise measurements (or constraints) from MEG and Mu2e: the comparison between these determinations will help pinning down the underlying theory.

Example of interplay between MEG and Mu2e is shown for the Scalar Leptoquark searches. In Fig. 2*a*, the reach for the new coupling λ, as defined from eq. 14 of [7], is reported for a range of Scalar Leptoquark masses for both MEG upgrade and conversion experiments. The compilation is extracted from the Mu2e TDR. It is clear that while not excluding the Leptoquark existence at few TeV masses, the CLFV coverage extends up to masses of O(100 TeV). Another example is provided by the Left-Right symmetric models that is a BSM theory useful to restore parity at short-distances. A recent study [8] predicts the CLFV rates in this environment assuming a new mass breaking scale at around 5 TeV. The correlation between the BR for the MEG upgrade and $R_{\mu e}$ for the conversion experiments are shown in Fig. 2*b*. It is clear that the two experiments can cover the expectations for the full phase space of this theory. The ratio of the two measurements will help constraining it.

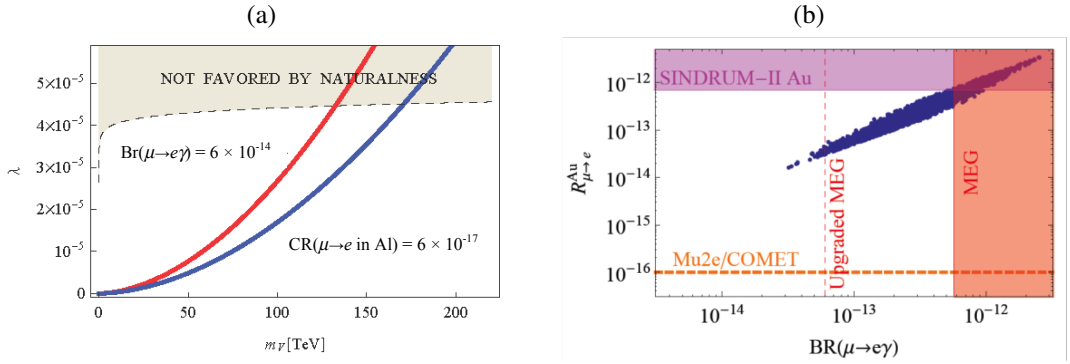

Figure 2. (*a*) Reach acheavable in the Scalar Leptoquark search for the MEG upgrade and Mu2e as a function of the coupling λ and the Scalar Leptoquark mass. (*b*) Expected BR and $R_{\mu e}$ for Left-Right symmetric models for the MEG upgrade and the muon conversion experiments.

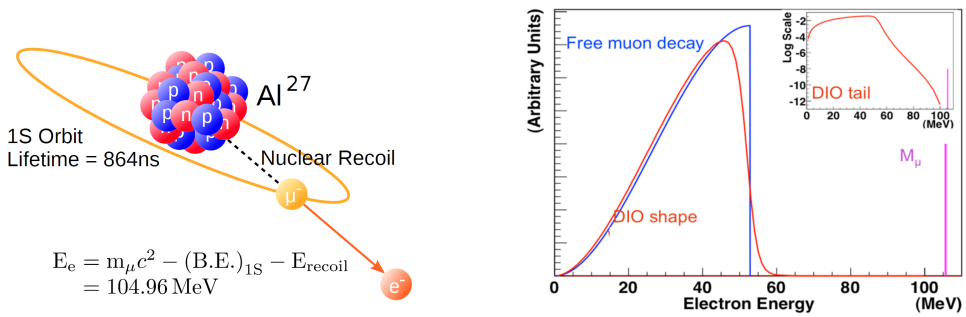

Figure 3. (Left) sketch of the muon to electron conversion process. (Right) Energy spectrum for electrons coming from muon decay in orbit. Perfect resolution is assumed. The spectrum is a modified Michel spectrum with a long tail that falls quickly as $(E_e - E_{endpoint})^5$ in proximity to the kinematic endpoint.

2 Mu2e: search for μ to e conversion at Fermilab

The measurement of the neutrinoless μ^- to e^- conversion rate, in presence of a nucleus, is defined relatively to the ordinary capture of the muon on the nucleus as follows:

$$R_{\mu e} = \frac{R(\mu^- + A(Z,N) \rightarrow e^- + A(Z,N))}{R(\mu^- + A(Z,N) \rightarrow \nu_\mu + A(Z-1,N)}). \quad (1)$$

The *conversion signal*, CE, consists of a monoenergetic electron (see Fig. 3.left) close to the muon mass, once corrected for binding energy and nuclear recoil, that has to be separated by means of high momentum resolution from the spectrum of the electrons produced in the *muon decay in orbit* process, DIO (see Fig. 3.right). The stopped muons have a large chance of decaying when orbiting around the nucleus and their spectrum is substantially modified from the free decay by the presence of a large recoil tail that falls rapidly as the energy approaches the kinematical endpoint.

However, in Sindrum-II additional background sources were dominating. In particular, after rejection of cosmics, a prompt background coming from *radiative pion capture*, RPC, $\pi + N \rightarrow \gamma^* + N'$, was found to be the most resistant background. In this process, the electron positron pair, produced either by internal or external conversion, becomes a source of CE candidate when the e^- momentum gets in the right selection window. These observations have driven the design strategy of the new generation of experiments for the muon to electron conversion, as Mu2e. The Mu2e goal is to achieve a single CE event sensitivity of 2.5×10^{-17} or constrain the R_μ value to be below 6×10^{-17} at 90% C.L., that is four orders of magnitude better than the previous best limit.

There are four ingredients to achieve this: (i) *An high intensity muon beam*. The goal is to increase of a factor of four the nowadays muon intensity on target to 10^{11}/sec. This can be achieved by means of high muon production on target and a curved solenoidal system to allow for charge and momentum selection. The solenoidal system creates a selective transport channel that increases intensity while reducing the associated needs for beam power (compare 1 MW at PSI for Sindrum-II and 8 kW for Mu2e). (ii) *A pulsed beam structure*. This allows to reject the prompt background. The target has to be selected in a way that the muon lifetime, τ_μ, in the bound system is smaller than the bunch period. Mu2e has selected an aluminum target (τ_μ = 864 ns) that well matches with the bunch structure of the Fermilab accelarator complex. For the beam delivered to Mu2e, the micro-bunch structure will be of 1684 ns. The trick is to wait for the *beam-flash* of particles travelling with the transported beam to disappear as well as waiting for the most relevant prompt backgrounds to decay. The start of the data acquisition is tipically set at ~ 700 ns after the bunch arrival time. (iii) The out of time particles travelling with the beam have to be negligible. This is referred to as the *proton extinction requirement*. Calculation by full simulation has shown that to suppress the prompt backgrounds generated by beam electrons, muon decay-in-flight, pion decay-in-flight and RPC requires a pulsed beam where the ratio of beam between pulses to the beam contained in a pulse is below 10^{-10}. (iv) *A redundant high-precision detector* has to analize the capture products to separate CE and DIO spectra and reduce to negligible contribution the additional background sources.

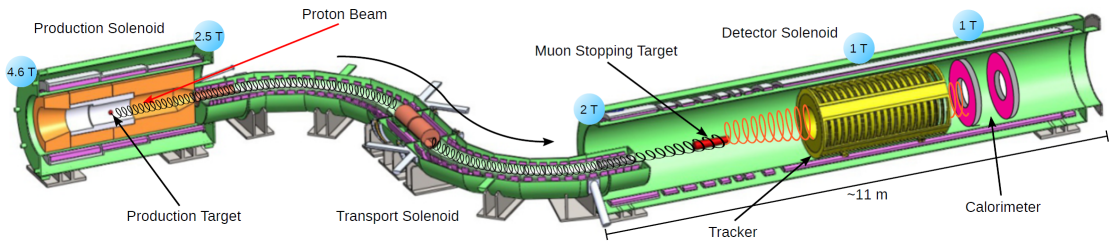

Figure 4. Layout of the Mu2e experiment.

2.1 The Mu2e detector layout

The layout of the Mu2e experiment is shown in Figure 4. An array of superconducting solenoids forms a graded magnetic system constituted by a Production Solenoid, PS, a Transport Solenoid, TS, and a Detector Solenoid, DS.

The PS contains the tungsten production target that intercepts an 8 GeV pulsed proton beam brought, by means of a dedicated beam-line, from the Fermilab delivery ring. The gradient field in

the PS increases from 2.5 to 4.6 Tesla in the same direction of the incoming beam and opposite to the outgoing muon beam direction. This gradient field works as a magnetic lens to focus low energy particles into the transport channel. The focused beam is constituted by muons, pions and a small number of protons and antiprotons. The S-shaped Transport Solenoid transfers efficiently low energy negative charge particles to the end of the beam-line while allowing for a large fraction of the pions to decay to muons. A collimator in the middle section attenuates nearly all positively charged particles. The antiproton residual background is reduced by inserting a special absorber in the middle section. The DS presents a graded field from 2 to 1 Tesla in the upstream region where the stopping target resides. This lens increases the acceptance for CE while helps rejecting beam-related backgrounds. A uniform magnetic field of 1 Tesla resides in the region of the tracker and calorimeter systems. Around 50% of the muon beam is stopped by the target while the surviving beam is dumped at the end of the cryostat. The DS is covered externally by a Cosmic Ray Veto system.

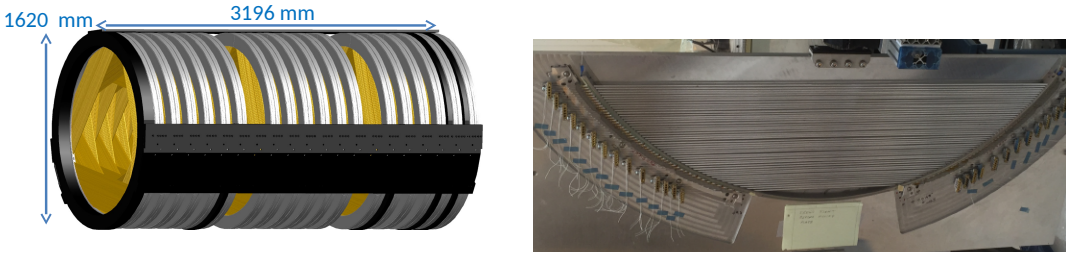

Figure 5. (Left) Sketch of the Mu2e straw tracker system. (right) Picture of the first prototype built for straw tube panel.

When muons stop in the aluminum target, they are captured in an atomic excited state. They prompty fall to the ground state: 39% decay in orbit while 61% are captured on the nucleus. Low energy photons, neutrons and protons are emitted in the nuclear capture process and constitutes an environmental background that produces a ionization dose and a neutron fluence on the detection systems as well as an accidental occupancy for the reconstruction program. This background is fully simulated in overlap with the signals coming from the apparatus.

The tracking detector is made by low mass straw drift tubes oriented transversally to the solenoid axis. The detector consists of about 20000 straw tubes arranged in 18 station, as shown in Fig. 5.left. Each tube is of 5 mm in diameter and contains a 25 μm sense wire. The straw walls are made out of Mylar and have a thickness of 15 μm. The coordinate along the straw is done by time division. The gas used is a 80:20 mixture of Argon-CO_2. The tracker is around 3 m long and placed inside a 1 T uniform magnetic field. It measures the momenta of the charged particles from the reconstructed trajectories using the hits detected in the straw. A circular inner hole inside the tracker allows it to be insensitive for charged particle momenta below 55 MeV/c. The tracking preparation proceeds well. In Fig. 5.right, an example of the first panel prototype built is shown.

The electromagnetic calorimeter system [9] is composed by two disks of scintillating crystals and is placed downstream of the tracker. Each disk is made of about 900 BaF_2 crystals, each readout by two *solar blind* UV extended avalanche photo-diodes (APD). In Fig. 6.left. a drawing of these two disks is shown. Similarly to the tracker, the inner circular hole allows to be insensitive to the DIO electrons up to 55 MeV/c momenta. The calorimeter tasks are that of providing a powerful particle identification between muons and electrons, an independent trigger system and a seed for tracking

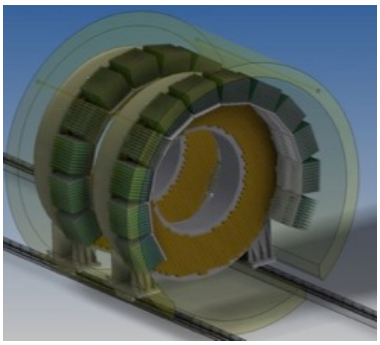

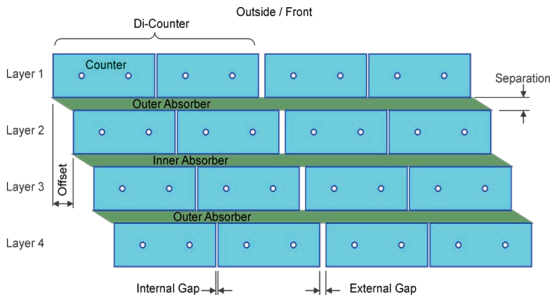

Figure 6. (Left) CAD drawings of the calorimeter disks. Calorimeter innermost (outermost) radius is of around 350 mm (670 mm). Crystal length of 200 mm. Layout of the FEE and digitization crates is also shown. (Right) Schematic drawing of the cross-sectional view of a CRV counter. Each counter is 20 mm thick, with a width of 50 or 60 mm. Length up to 6.6 m.

in a complicated reconstruction environment. In order to fulfill these requirements, the calorimeter has to provide an energy resolution of O(5%), a time resolution < 500 ps and a position resolution better than 1 cm for 100 MeV electrons. The selected crystals should also be able to survive a dose of 100 krad and a fluence of up to 10^{12} n/cm^2. The photosensors are somehow shielded by the crystals themselves and should only sustain a fluence up to 3×10^{11} n_{1MeV}/cm^2. Prototypes for the solar blind APDs have been developed but the dark noise is still too high and cooling them down to -10° C is needed. Backup options are being explored.

One major background source for Mu2e is related to cosmic ray muons faking CE when interacting with the detector materials. These events occur at a rate of $\sim$ one/day. In order to reduce their contributions to below 0.1 event in the experiment lifetime, the external area of the DS (and a part of the TS) are covered by a Cosmic Ray Veto, CRV, system. Requirements for the system is to get a vetoing efficiency of at least 99.99% for cosmic ray tracks while withstanding an intense radiation environment. The basic element of the CRV is constituted by four staggered layers of scintillation counters (see Fig. 6.right) each having two embedded Wavelength Shifting Fibers readout by means of 2×2 mm^2 SiPM from Hamamatsu. Test beams on full size prototype have been carried out.

Further instrumentation exists, such as the monitor to measure the proton beam extinction and a High Precision Germanium detector to monitor the stopping rate in the aluminum target. The latter one is needed to provide the normalization for the $R_{\mu e}$ conversion rate. Further information can be found in ref. [5] .

2.2 Reconstruction of CE candidates

At this energy the momentum resolution is dominated by fluctuations in the energy loss in the target, by multiple scattering and by bremsstrahlung in the tracker. By performing a full simulation of the tracker, a pattern recognition and a Kalman fitter for the tracking we obtain: a CE reconstruction efficiency of 9 % for good quality tracks and at least 25 hits/track. The resolution is well parametrized by a Crystal Ball function with a negative bremsstahlung tail, a Gaussian core of 116 keV and a long exponential positive resolution tail. This result is obtained in a kind of hostile environment due to the large production of neutrons, photons and protons from the muon capture processes. Note that

the muon stopping rate needed to arrive to the final goal of 6×10^{17} stopped muons is of around 10 GHz. In Fig. 7.left, an example of 1 single micro-bunch event in the tracker is shown. This has been obtained with a Geant-4 simulation displaying all hits generated by the environmental background. The irreducible background is provided by the DIO electrons that have to be distinguished by the mono-energetic CE. The finite tracking resolution and the positive reconstruction tail has a large effect on the falling spectrum of the DIO background that translates in a residual contamination in the signal region. Fig. 7.right shows the signal and background distributions as seen by a full simulation of the experiment (pileup included) in the following conditions: (i) 3.6×10^{20} proton on target, (ii) a corresponding number of 6×10^{17} muon stops and (iii) a $R_{\mu e}$ of 10^{-16}. After maximizing signal over background, the best selection corresponds to count events in a momentum window between 103.75 and 105 MeV/c. A DIO contribution of 0.199 events is estimated and 3.5 candidates are observed. Estimate of other backgrounds are presented in Tab.3 for a total background contribution of 0.37 events. This counting corresponds to set a limit on $R_{\mu e}$ below 6×10^{-17} at 90 % C.L., in good agreement with the experiment design goal. A very important step for this measurement is the tracker calibration. To accurately predict the DIO rate, we should calibrate the tracker momentum i.e. determine the shifts, the scale and the resolution of the measured momentum compared to the true one. After a basic calibration based on construction and installation survey data, the calibration will be based both on the usage of the lower momentum high statistic DIO sample itself and on independent processes of low energy two body decay, such as the one from stopped π^+ on target undergoing the $\pi \to e\nu$ decay. Selecting the positive pions will help to avoid nuclear capture but asks for reversing the momentum selection in the TS. Moreover, the data have to be collected at shorter rate and an extrapolation from lower energies to the conversion endpoint is needed.

2.3 Experiment status and schedule

At the moment of writing, the Mu2e experiment has succesfully completed the CD-2 review for all systems and the CD-3 reviews for the superconducting cables, the civil construction and the Transport Solenoids.

The heart of the Mu2e apparatus is provided by the superconducting magnetic system whose design, fabbrication, assembly and commissioning drives the experiment schedule. The magnet status is satisfactory. The construction and testing of the superconducting cables proceeds well. The international bid for the DS and PS have been concluded and the construction phase for the large magnets are started at General Atomics, San Diego, USA. For the TS, a prototype of one module have been built by ASG Superconducting in Genova in collaboration with the INFN group of Genova. Tests and quality control of the prototype have been carried out this summer with satisfactory results. The bid on the TS have also been completed and has been assigned to the ASG. The ground breaking cerimony for the experimental hall has been held on April 2015. Since then the civil construction is proceeding at a real fast pace. Completion of CD-3 for the apparatus and for the accelerator are expected to happen in summer 2016. This will start the construction for the detectors and for the accelerator. The schedule foresees a completion of the installation and commissioning with beam at the end of 2020.

3 Conclusions and perspectives

The Mu2e experiment design and construction proceeds well and it is on schedule to be commissioned with beam for the end of 2020. Its goal is to probe CLFV with a single event sensitivity of 2.5×10^{-16} or set an upper limit on the conversion rate $< 6 \times 10^{-17}$ at 90 % C.L. improving of four orders of magnitude the previous sensitivity. For the long term future (> 2025) the possibility of a Mu2e phase-2, is being explored with the goal of increasing the sensitivity of an additional factor of 10. This can

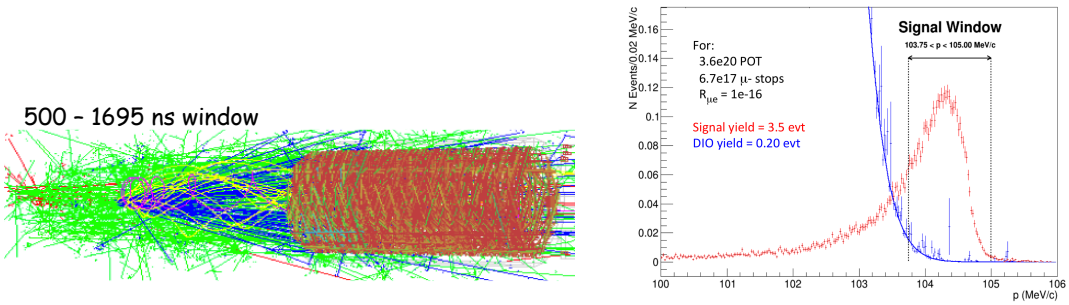

Figure 7. (Left) event display of a single micro-bunch event. (Right) full simulation of DIO and CE events for an assumed $R_{\mu e}$ of 10^{-16}.

Category	Background process	Estimated Yield (events)
Intrinsic	Decay in orbir (DIO)	0.199 ± 0.092
	Muon Capture (RMC)	0.000 ± 0.004
Late Arriving	Pion capture (RPC)	0.023 ± 0.006
	Muon decay in flight	< 0.003
	Pion decay in flight	0.001 ± 0.001
	beam electrons	0.003 ± 0.001
Miscellaneous	pbar	0.047 ± 0.024
	Cosmic rays	0.092 ± 0.020
	Total	0.37 ± 0.10

Table 1. Expected background list as evaluated by full simulation as extracted by the Mu2e TDR

be obtained aiming to get a higher beam intensity and a detector that whitstands this intensity and is able to handle the accidental activity coming from muon capture. In this context, only the option based on the new Proton Improvement Plan, PIP-2, [10] is being studied.

References

[1] S.M.Bilenky et al., *Phys. Lett.* **B67**, 309 (1977)
[2] F.Grancagnolo et al., *Nucl.Phys.Proc.Supp.* **248-250** 1-146 (2014).
[3] The MEG collaboration,*Phys.Rev.Lett.* **110** 201801 (2013).
[4] The SINDRUM II Collaboration, *Eur.Phys.J.* **C47** 337-346 (2006)
[5] The Mu2e Collaboration, *FERMILAB-TM-2594*, **ArXiv:1501.05241** (2015).
[6] A. De Gouvea et al., *Prog. Part. Nucl. Phys* **71** 75-92 (2013).
[7] J.M.Arnold et al., *Phys.Rev* **D88** 035009 (2013).
[8] C.H.Lee et al., *Phys.Rev* **D88** 092010 (2013).
[9] X.. et al., *Nucl. Instr. and Meth.* **A5857**, 10.1016/j.nima.2015.09.074.
[10] http://pip2.fnal.gov.